ADVANCED FUNCTIONAL MATERIALS

FULL PAPER

DOI: 10.1002/adfm.200500523

Amorphous Diphenylaminofluorene-Functionalized Iridium Complexes for High-Efficiency Electrophosphorescent Light-Emitting Diodes**

By *Wai-Yeung Wong*,* *Gui-Jiang Zhou*, *Xiao-Ming Yu*, *Hoi-Sing Kwok*, and *Ben-Zhong Tang*

Two new phosphorescent iridium(III) cyclometalated complexes, [Ir(DPA-Flpy)$_3$] (**1**) and [Ir(DPA-Flpy)$_2$(acac)] (**2**) ((DPA-Flpy)H = (9,9-diethyl-7-pyridinylfluoren-2-yl)diphenylamine, Hacac = acetylacetone), have been synthesized and characterized. The incorporation of electron-donating diphenylamino groups to the fluorene skeleton is found to increase the highest occupied molecular orbital (HOMO) levels and add hole-transporting ability to the phosphorescent center. Both complexes are highly amorphous and morphologically stable solids and undergo glass transitions at 160 and 153 °C, respectively. These iridium phosphors emit bright yellow to orange light at room temperature with relatively short lifetimes (< 1 μs) in both solution and the solid state. Organic light-emitting diodes (OLEDs) fabricated using **1** and **2** as phosphorescent dopant emitters constructed with a multilayer configuration show very high efficiencies. The homoleptic iridium complex **1** is shown to be a more efficient electrophosphor than the heteroleptic congener **2**. Efficient electrophosphorescence with a maximum external quantum efficiency close to 10 % ph/el (photons per electron), corresponding to a luminance efficiency of ~ 30 cd A^{-1} and a power efficiency of ~ 21 lm W^{-1}, is obtained by using 5 wt.-% **1** as the guest dopant.

1. Introduction

Organic light-emitting diodes (OLEDs) based on phosphorescent third-row heavy-metal complexes continue to spark a flurry of research activities in the scientific community due to the potential application of these compounds as highly efficient electroluminescent emitters.[1] Both electrogenerated singlet and triplet excitons can be harvested for light emission in these complexes (usually referred to as "triplet harvesting"), with the internal quantum efficiency of phosphorescent emitters theoretically approaching 100 %.[2] The highly efficient phosphorescence emission is attributed to the strong spin-orbit coupling of the electronic states by the heavy-atom effect of the metal, which can facilitate the singlet–triplet spin crossover. Of all the transition metals that have been employed as emissive traps or dopant emitters in electroluminescent devices (iridium,[3] platinum,[4] osmium,[5] and more recently, ruthenium[6]), Ir^{III} complexes are still the most effective. Both the electroluminescence (EL) efficiency and the emission wavelength of iridium-based devices are greatly influenced by the organic ligand chromophore, which is generally a mono-anionic derivative of bidentate *o*-pyridylarene or *o*-pyridylheterocycle (abbreviated as N-C).[7] Although red-, green-, and blue-light-emitters with excellent color purity and sufficient luminous efficiency are required for full-color display applications, there is also a great demand for emitters that afford a bright color, such as yellow, orange or light blue, for multiple-color displays.[8]

Recent research endeavors along this line have involved the use of fluorene-based chromophores, which possess great promise as highly stable and efficient emissive cores in the synthesis of useful iridium complexes.[9] One advantage of fluorene-bridged materials for some applications is the ease of functionalization of the fluorene 9-position.[10] However, all related work reported previously has been restricted exclusively to polymer-based devices, where the fluorene-based phosphor is processed with a polymer host by the spin-coating method.[9] It is also known that a large hole-injection (HI) barrier for organic, fluorene-containing molecules often limits their device efficiency. In view of the fact that most of the hole-transporting (HT) molecular glasses reported so far are built mainly from aromatic amines,[11] we envision that triarylamines or their derivatives can be incorporated into the fluorene nucleus to improve the HI/HT properties and morphological

[*] Dr. W.-Y. Wong, Dr. G.-J. Zhou
Department of Chemistry and
Centre for Advanced Luminescence Materials
Hong Kong Baptist University
Waterloo Road, Kowloon Tong, Hong Kong (P.R. China)
E-mail: rwywong@hkbu.edu.hk
X.-M. Yu, Prof. H.-S. Kwok
Department of Electronic and Electrical Engineering and
Centre for Display Research
The Hong Kong University of Science and Technology
Clearwater Bay, Hong Kong (P.R. China)
Prof. B.-Z. Tang
Department of Chemistry and Centre for Display Research
The Hong Kong University of Science and Technology
Clearwater Bay, Hong Kong (P.R. China)

[**] This work was supported by a CERG Grant from the Hong Kong Research Grants Council (HKBU2022/03P) and a Faculty Research Grant from the Hong Kong Baptist University (FRG/04-05/II-59).

ADVANCED FUNCTIONAL MATERIALS

stability.[12] This prompted us to design new ligand systems for Ir^{III} complexes with good amorphous properties and improved functional properties. Interestingly, there have not been any reports to date exploring arylamine-substituted fluorene-based Ir^{III} phosphors for small-molecule OLEDs. Here, we report the synthesis, redox, photophysical, and EL properties of two bifunctional bis- and tris-cyclometalated Ir^{III} complexes containing diphenylaminofluorene units in which the HT and electroluminescent functional groups are integrated into one molecular unit essential for more efficient charge transport in the EL process. We demonstrate that the diphenylamino moiety end-capped onto a highly luminescent fluorene backbone can offer a good path towards lowering the ionization potential, inducing morphologically stable amorphous thin-film formation, and enhancing the thermal stability of the complexes.

2. Results and Discussion

2.1. Preparation and Characterization

Scheme 1 shows the synthetic protocol for the new iridium complexes **1** and **2**. The key compound in our studies is the cyclometalating ligand [H(DPA-Flpy)], obtained from the Stille coupling of (7-bromo-9,9-diethylfluoren-2-yl)diphenylamine[13] with 2-(tributylstannyl)pyridine. The design rationale of [H(DPA-Flpy)] is that it possesses both the diphenylamino moiety as the HT unit and the 2-phenylpyridine group as a cyclometalating site. The homoleptic Ir^{III} complex **1** was obtained by direct thermal reaction of $[Ir(acac)_3]$ (Hacac = acetylacetone) with [H(DPA-Flpy)] in refluxing glycerol. The heteroleptic Ir^{III} compound **2** was synthesized in two steps from the cyclometalation of $IrCl_3 \cdot nH_2O$ with [H(DPA-Flpy)] to initially form the chloride-bridged dimer $[Ir(DPA\text{-}Flpy)_2Cl]_2$, followed by treatment with acetylacetone in the presence of Na_2CO_3.[14] Purification of the mixture by silica chromatography provided **1** and **2** as air-stable orange powders of high purity. All the new compounds were fully characterized by NMR spectroscopy and fast-atom-bombardment mass spectrometry (FAB-MS) and shown to consist of well-defined structures. The first-order ^1H and ^{13}C NMR spectra of **1** are consistent with a facial geometry around the Ir center, which indicates that the number of coupled spins is equal to that of the protons on one ligand, because the three N-C ligands are magnetically equivalent owing to the inherent C_3 symmetry of the complexes. The parent ion peaks at $m/z = 1589$ and 1222 (m/z: mass/charge) in the FAB mass spectra of **1** and **2**, respectively, confirm the identities of both complexes.

2.2. Photophysical and Thermal Properties

The decomposition temperature was determined from thermogravimetric analysis (TGA) measured under a nitrogen stream (Table 1). The thermal-stability data reveal that both complexes have excellent thermal stability and their 5 % weight-reduction temperatures ($\Delta T_{5\,\%}$) are significantly different: 473 °C for **1**, 432 °C for **2**, and only 243 °C for $[Ir(acac)_3]$. Thus, complex **1** is thermally more stable than complex **2**. In addition, both complexes were found to sublime before their decomposition temperatures were reached. Differential scanning calorimetry (DSC) data of **1** and **2** showed no crystallization and melting peaks but only glass-transition temperatures (T_g). Both compounds showed a very high T_g value, in excess

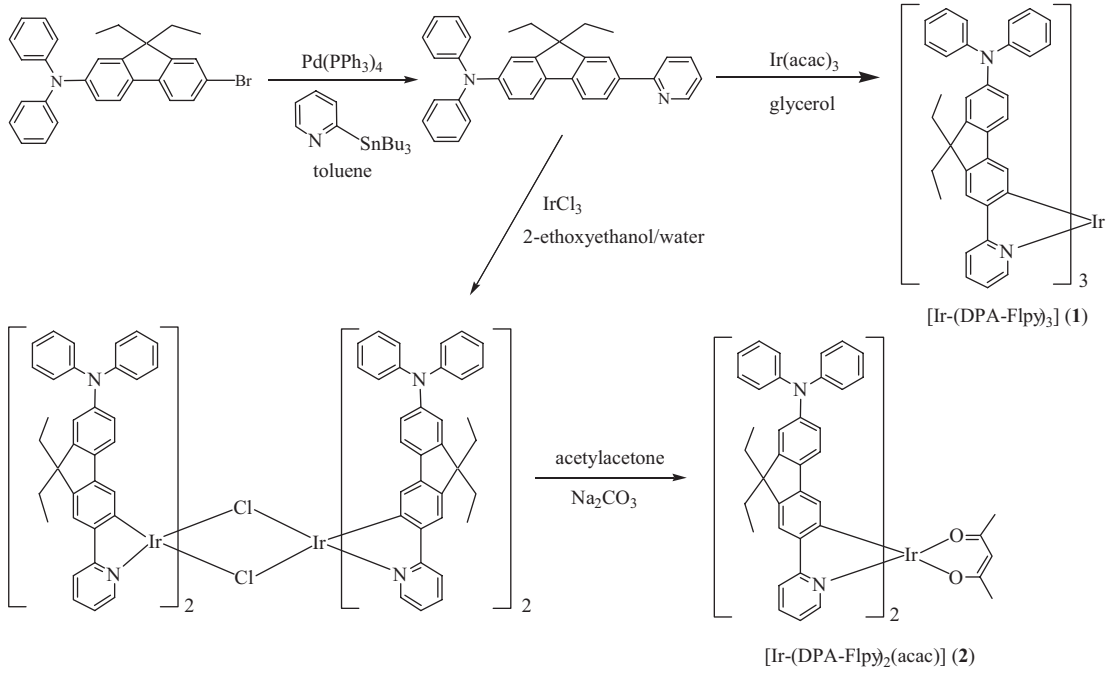

Scheme 1. The synthetic routes to iridium complexes **1** and **2**.

Table 1. Photophysical and thermal data for **1** and **2**. (Φ_P: phosphorescence quantum yield; τ_P: phosphorescence lifetime; k_r and k_{nr}: radiative and non-radiative rate constants, respectively.)

	Absorption (293 K)	Emission (293 K)							$\Delta T_{5\%}$ [°C]	T_g [°C]
	λ_{abs} [nm] [a] CH_2Cl_2	λ_{em} [nm] CH_2Cl_2	λ_{em} [nm] Film	Φ_P [b]	τ_P [μs] [c]	k_r [s^{-1}]	k_{nr} [s^{-1}]	τ_P [μs] [d]		
1	309 (4.86) 375 (4.91) 415 (4.74) 478sh (3.97)	555, 595sh	567, 607sh	0.12	0.08 (0.67)	1.5×10^6	1.1×10^7	0.08 (0.55)	473	160
2	297 (4.70) 387 (4.70) 408sh (4.68) 478sh (3.84)	564, 607sh	575, 622sh	0.13	0.11 (0.85)	1.2×10^6	7.9×10^6	0.05 (0.61)	432	153

[a] logε values are shown in parentheses. sh = shoulder. [b] Measured in degassed CH_2Cl_2 relative to *fac*-[Ir(ppy)$_3$] ($\Phi_P = 0.40$), $\lambda_{ex} = 380$ nm. [c] In degassed CH_2Cl_2 at 293 K. The radiative lifetimes τ_r (μs) are shown in parentheses. [d] For a solid film at 293 K. Numbers in parentheses were obtained at 77 K.

of 150 °C, and exist as highly amorphous solids that are resistant to crystallization. Usually, an amorphous film with a higher T_g is desirable for OLEDs with high stability and efficiency. While the parent unsubstituted complex [Ir(Flpy)$_3$] (H(Flpy) = 2-(9,9-dimethylfluoren-2-yl)pyridine) only possesses a T_g of 98 °C,[15] our results suggest that the diphenylamino moieties play a pivotal role in improving the amorphous nature of the phosphor molecules, leading to materials of high T_g values. This would give rise to new iridium complexes with improved compatibility between the phosphorescent dopant and the organic host, and eventually lead to highly efficient, electrophosphorescent, small-molecule OLEDs.

Figure 1 depicts the UV-vis and photoluminescence (PL) spectra of **1** and **2**. The spectroscopic data of **1** and **2** are listed in Table 1. The intense absorption bands (logε ~ 4.7–4.9) at

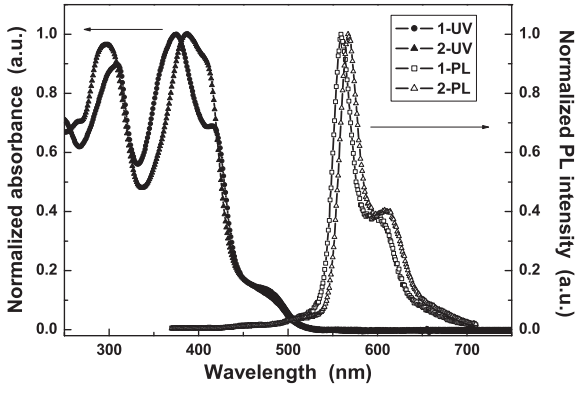

Figure 1. Optical absorption and photoluminescence spectra of **1** and **2** in CH_2Cl_2 at 293 K.

ca. 309–375 nm for **1** and ca. 297–387 nm for **2** appear to be ligand-based transitions that closely resemble the spectra of the free ligand HN-C ($\lambda_{abs} = 301$, 372 nm), and are attributed to the spin-allowed $^1\pi$–π^* transitions associated with the arylamino and aminofluorenyl fragments. Similar absorption features were observed by Low et al. in the spectra of Ar_2N–C_6H_4–X compounds near 300 and 350 nm.[16] The bands are also accompanied by weaker, lower-energy features extending into the visible region from 410 to 480 nm that correspond to excitation to ^{1}MLCT (metal–ligand charge transfer), ^{3}MLCT and $^3\pi$–π^* states. Observation of the ^{3}MLCT and $^3\pi$–π^* bands confirms strong spin-orbital coupling between the singlet and triplet manifolds. With reference to previous spectroscopic data for [Ir(Flpy)$_3$] and other similar iridium complexes in the literature,[17] complexes **1** and **2** probably possess the dominantly $^3\pi$–π^* lowest-excited states. While the ligand emits an intense fluorescence at 446 nm, both iridium complexes show strong room-temperature phosphorescence (λ_{em} in CH_2Cl_2 = 555 and 564 nm for **1** and **2**, respectively) from the predominantly ligand-centered $^3\pi$–π^* excited state, which display large Stokes shifts (> 100 nm). The vibronic splitting at ca. 1165 cm^{-1} (ν_{0-1}) in the emission profile corresponds to the aromatic stretching of the cyclometalated ligands, which is diagnostic of the involvement of the intraligand π–π* transitions in the emission, and these vibronic fine structures preclude the assignment of ^{3}MLCT states, which are usually broad and featureless. Both the absorption and phosphorescence spectra of **1** are located at wavelengths ($\lambda_{abs} = 375$, 415, 478 nm, $\lambda_{em} = 555$ nm) longer than those of [Ir(Flpy)$_3$] without the diphenylamino units ($\lambda_{abs} = 321$, 336, 405 nm, $\lambda_{em} = 545$ nm).[17] The introduction of an electron-donating diphenylamino group into the electron-deficient pyridine moiety of the ligand is expected to increase the donor–acceptor (D–A) character of the ligand. From these results, it can be concluded that the phosphorescence spectrum of **1** is red-shifted when their ligands have a larger π-conjugation space and/or strong intramolecular D–A interaction.[17] Tris-chelate complex **1** has a very similar emission pattern to its relative **2** with the same N-C ligand. The phosphorescence quantum yields, Φ_P, in degassed CH_2Cl_2 solutions excited at 380 nm are moderate at 0.12 and 0.13 for **1** and **2**, respectively, relative to a *fac*-[Ir(ppy)$_3$] standard ($\Phi_P = 0.40$, Hppy = 2-phenylpyridine).[18] The emission lifetimes in solution and solid were measured and found to be well fitted to a single-exponential decay. The observed phosphorescence lifetimes, τ_P, have a magnitude of about 0.08–0.11 μs in CH_2Cl_2, shorter than those of [Ir(Flpy)$_3$] (1.2 μs)[17] and most of the

other reported complexes of this kind. Accordingly, the radiative lifetimes (τ_r) of the triplet excited state deduced from $\tau_r = \tau_P/\Phi_P$ are as short as 0.67–0.85 μs,[3k] which correlates well with the unusually large extinction coefficients measured for the ^{3}MLCT bands. In the solid state, the lifetime is even shorter (0.05–0.08 μs), possibly due to the phosphorescence self-quenching associated with molecular packing. The τ_P values at 77 K are 6–7 times longer than those at 293 K. The similarity of the phosphorescence quantum yields and lifetimes for these two complexes is consistent with emission predominantly from the "$(N\text{-}C)_2Ir$" fragment. The triplet radiative and non-radiative rate constants, k_r and k_{nr}, are calculated from Φ_P and τ_P using the relationships $\Phi_P = \Phi_{ISC}(k_r/(k_r + k_{nr}))$ and $\tau_P = (k_r + k_{nr})^{-1}$. Here, Φ_{ISC} is the inter-system-crossing yield, which can be safely assumed to be 1.0 for iridium complexes because of the strong spin-orbit interaction caused by the heavy-atom effect of iridium. In fact, no fluorescence could be detected for either complex at 293 or 77 K. Complexes **1** and **2** have similar k_r values, as can be expected from the comparable quantum efficiencies and lifetimes of both compounds. Also, it is found that the k_r value for **1** (1.5×10^6 s^{-1}) is larger than that found for $[Ir(Flpy)_3]$ (2.5×10^5 s^{-1}), and this would be advantageous to the design of highly efficient devices based on light-energy harvesting from the triplet excitons.

2.3. Electrochemical and Electronic Characterization

The electrochemical properties of **1** and **2** were examined by cyclic voltammetry (Table 2). Both complexes show two reversible anodic redox couples with potentials in the range 0.15–0.53 V, and these oxidation waves correspond to the sequential removal of electrons from the peripheral arylamino group and Ir-phenyl center to form radical cations and dications, respectively. The reversible reduction occurs primarily on the heterocyclic portion of the N-C ligand with potentials ranging from –1.67 to –1.87 V, typical of phenylpyridyl-based chromophores in similar complexes. The homoleptic complex **1** has a reduction potential ca. 200 mV more negative than its heteroleptic derivative **2**. Notably, the incorporation of NPh_2 groups to the fluorene core caused a negative shift in the anodic half-wave potential ($E_{1/2}$) by ca. 80 mV, as observed by changing from the unsubstituted complex (+0.23 V) to **1**. On the basis of the redox data, we estimated the highest occupied molecular orbital (HOMO) and lowest unoccupied molecular orbital (LUMO) energy levels of **1** and **2** with reference to the energy level of ferrocene (4.8 eV below the vacuum level), and the first oxidation potentials were used to determine the HOMO energy levels.[19] The HOMO and LUMO levels for **1** and **2** closely match the energy levels for 4,4′-bis[*N*-(1-naphthyl)-*N*-phenylamino]biphenyl (NPB, HOMO: –5.2 eV) and 2,2′,2″-(1,3,5-phenylene)tris(1-phenyl-1*H*-benzimidazole) (TPBI, LUMO: –2.9 eV). The LUMO levels of both complexes (–2.93 and –3.13 eV) are lower than that of 2-(4-biphenylyl)-5-(4-*tert*-butylphenyl)-1,3,4-oxadiazole (PBD, –2.4 eV),[8a] one of the most widely used hole-blocking/electron-transport (HB/ET) materials, and comparable to that of tris(8-hydroxyquinolinato)aluminum (Alq_3, –3.0 eV). When the diphenylamino end groups are attached to the fluorene rings, the HOMO value of **1** is raised to –4.95 eV relative to the vacuum level. Complex **1** shows elevated HOMO energy levels as compared to the unsubstituted complex (–5.02 eV), indicating that compound **1** is more electropositive (or has a lower ionization potential) than the non-NPh_2-capped analogue, and a better HT ability in **1** can therefore be expected.

Table 2. Electrochemical properties and frontier orbital energy levels of **1** and **2**.

Complex	$E_{1/2}^{ox}$ [a] [V]	$E_{1/2}^{red}$ [a] [V]	HOMO [eV]	LUMO [eV]	E_g [b] [eV]
1	0.15, 0.45	–1.87	–4.95	–2.93	2.02
2	0.26, 0.53	–1.67	–5.06	–3.13	1.93

[a] 0.1 M $[Bu_4N]PF_6$ in CH_2Cl_2, scan rate 100 mV s^{-1}, versus Fc/Fc^+ couple. [b] E_g = LUMO – HOMO.

2.4. Electrophosphorescent OLED Characterization

Both organometallic phosphors have very good film- and glass-forming properties for evaluating their electrophosphorescent ability. Because of severe self-quenching in the solid, these phosphors are better used as a phosphorescent dopant rather than a single emission layer in OLEDs. OLED devices A–F were fabricated using **1** and **2** as emissive dopants with various doping concentrations. Complexes **1** and **2** are sufficiently stable with respect to sublimation for a fabrication process using a vacuum deposition method. Figure 2 shows the general four-layer structure for the electrophosphorescent devices and the molecular structures of the compounds used. 4,4′-*N*,*N*′-Dicarbazolebiphenyl (CBP) acts as a host material for the electrophosphor, NPB as the hole-transport layer, TBPI as both a hole-blocker and an electron-transporter, and LiF as an electron-injection layer. Here, TBPI was adopted for the devices to confine excitons within the emissive zone (instead of the commonly used 2,9-dimethyl-4,7-diphenyl-1,10-phenanthroline (BCP) or Alq_3) since it has a higher electron mobility.[20] We chose CBP as the host layer for device fabrication because of the excellent overlap of the UV-vis absorption of these iridium complexes with the PL spectrum of CBP, and such guest–host systems meet the requirement for efficient Förster energy transfer from the CBP host singlet to the iridium guest complexes. To optimize the device efficiency, a concentration dependence experiment was carried out in a range between 1 and 10 wt.-%. No emission from CBP was observed for >1 wt.-% doping ratios of both emitters even at high current density, indicating a complete energy transfer from the host exciton to the phosphor molecule. Key performance characteristics of the devices A–F are listed in Table 3. Figure 3 shows the EL spectra of these devices at a driving voltage of 8 V. We note that there is no voltage dependence of the EL spectra from 6 V to 12 V, and the maximum EL peak is independent of the guest concentration. Essentially, the de-

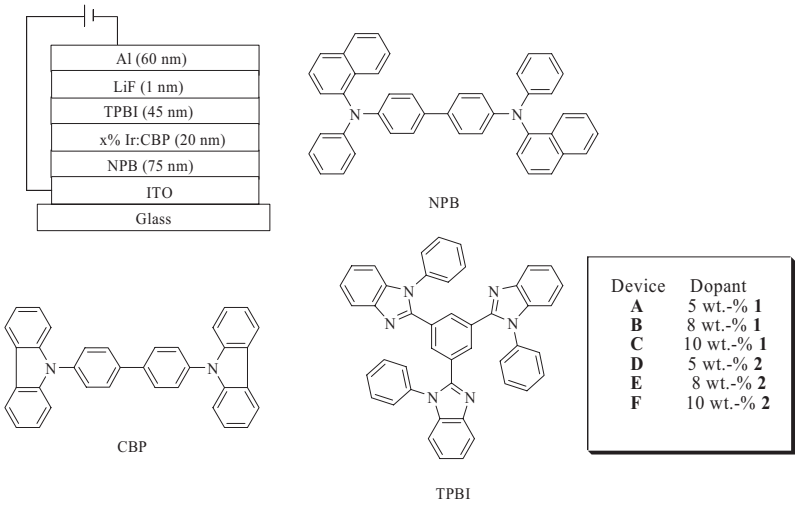

Figure 2. The general structure for OLED devices and the molecular structures of the relevant compounds used in these devices. TPBI: 2,2′,2″-(1,3,5-phenylene)tris(1-phenyl-1*H*-benzimidazole); CBP: 4,4′-*N*,*N*′-dicarbazolebiphenyl; NPB: 4,4′-bis[*N*-(1-naphthyl)-*N*-phenylamino]biphenyl; ITO: indium tin oxide.

Table 3. Performance of Ir-doped electrophosphorescent OLEDs.

Device	Phosphor dopant	$V_{turn\text{-}on}$ [V]	Luminance *L* [cd/m^2]	η_{ext} [%]	η_L [cd/A]	η_p [lm/W]	λ_{max} [d] [nm]
A	**1** (5 wt.-%)	4.2	2740 [a]	4.58	13.81	4.08	564
			8283 [b]	2.79	8.31	2.18	(0.50, 0.49)
			8283 (12) [c]	9.89 (4.5)	29.77 (4.5)	20.78 (4.5)	
B	**1** (8 wt.-%)	4.2	2570 [a]	4.36	13.02	4.56	564
			7621 [b]	2.60	7.74	2.12	(0.50, 0.49)
			7793 (11.5) [c]	8.23 (5.0)	24.73 (5.0)	15.54 (5.0)	
C	**1** (10 wt.-%)	3.8	2497 [a]	4.22	12.66	4.46	564
			7657 [b]	2.53	7.61	2.03	(0.50, 0.49)
			8314 (12) [c]	7.72 (4.5)	23.24 (4.5)	16.23 (4.5)	
D	**2** (5 wt.-%)	5.6	2158 [a]	4.25	10.42	3.06	572
			5720 [b]	2.34	5.72	1.34	(0.55, 0.45)
			8213 (12) [c]	7.89 (7.0)	19.26 (7.0)	11.22 (6.0)	
E	**2** (8 wt.-%)	4.6	1910 [a]	3.92	9.56	2.84	572
			5219 [b]	2.14	5.17	1.22	(0.55, 0.45)
			7673 (12) [c]	7.66 (5.0)	18.53 (5.0)	11.64 (5.0)	
F	**2** (10 wt.-%)	4.7	1305 [a]	2.79	6.71	1.91	572
			4010 [b]	1.68	3.90	0.92	(0.55, 0.44)
			6594 (12) [c]	5.78 (5.5)	13.65 (5.5)	8.45 (5.0)	

[a] Values collected at 20 mA cm^{-2}. [b] Values collected at 100 mA cm^{-2}. [c] Maximum values of the devices. Values in parentheses are the voltages at which they were obtained. [d] CIE coordinates [*x*,*y*] in parentheses.

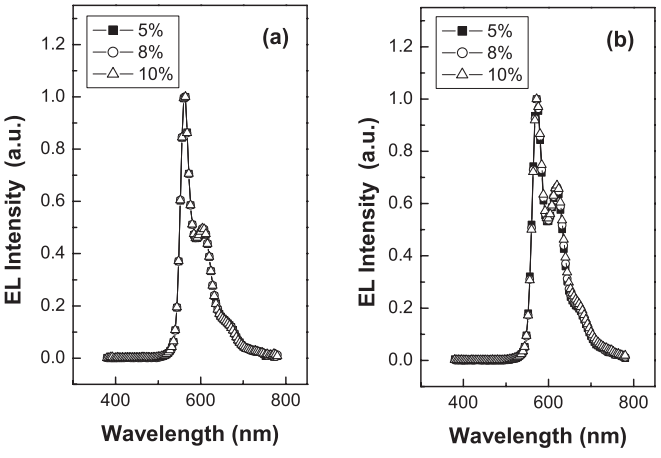

Figure 3. EL spectra of a) **1**- and b) **2**-doped OLEDs at different dopant concentrations.

vices A–C exhibit a strong yellow EL peak at about 564 nm with low turn-on voltages ($V_{turn\text{-}on}$) for light emission at 1 cd m^{-2} of 3.8–4.2 V and Commission Internationale de L'Eclairage (CIE) color coordinates of (0.50,0.49). The electroluminescent devices D–F containing dopant **2** turned on at ~5 V with a prominent EL emission at ~572 nm and CIE color coordinates at (0.55,0.45) correspond to the orange region of the CIE chromaticity diagram. In each case, the EL spectrum resembles its corresponding PL spectrum from the thin film, which indicates that both EL and PL arise from the same excited state or the same type of exciton. Moreover, there is no evidence of metal-complex aggregation.

The performance of these phosphorescence-based OLEDs is remarkable. Figure 4 presents current density and luminance versus bias voltage (*I*–*V*–*L*) curves of the Ir-doped OLEDs at three different doping concentrations (5, 8, and 10 wt.-%). In general, the brightness of the devices at a given current density

ADVANCED FUNCTIONAL MATERIALS

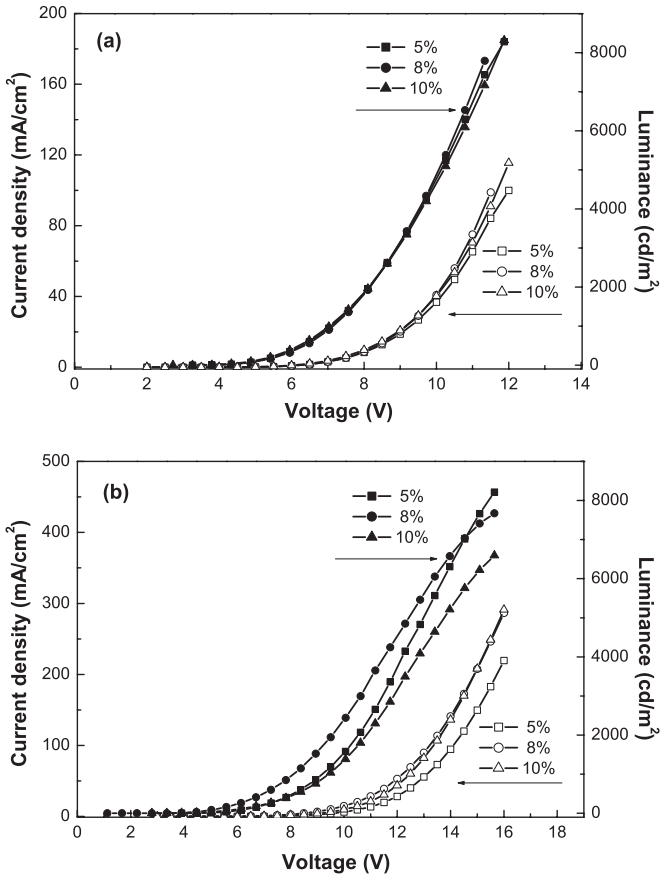

Figure 4. Current–voltage–luminance (*I–V–L*) characteristics of the electrophosphorescent OLED devices A–F with different dopant levels of a) **1** and b) **2**.

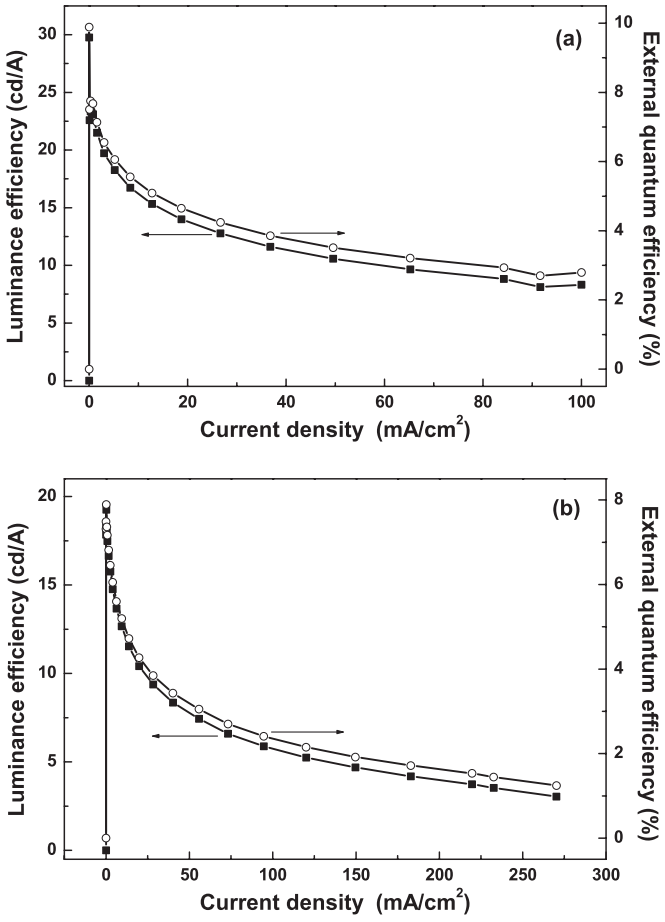

Figure 5. External quantum efficiency and luminance efficiency as a function of current density for OLED devices A and D using 5 wt.-% of guest dopants a) **1** and b) **2**.

tends to decrease slightly as the dopant concentration is increased from 5 to 10 wt.-% for each metal phosphor. The luminance reached 7793–8314 cd m^{-2} at 11.5–12.0 V for devices A–C, and 6594–8213 cd m^{-2} at 12.0 V for devices D–F. The external quantum and luminance efficiencies of the 5 %-doped devices as a function of current density for both complexes are depicted in Figure 5. Although the two Ir^{III} complexes have similar PL quantum yields and lifetimes in solution, the peak EL efficiencies of the devices fabricated from **2** are notably inferior to those of the [Ir(DPA-Flpy)$_3$]-based devices for a given doping level. We ascribe this higher efficiency to the more amorphous behavior of **1** (with a higher T_g), which shows improved chemical compatibility of **1** with the CBP host and leads to a more homogeneous distribution of this Ir dopant in CBP. Device A gave a maximum external quantum efficiency (η_{ext}) of 9.89 %, a luminance efficiency (η_L) of 29.77 cd A^{-1}, and a power efficiency (η_p) of 20.78 lm W^{-1} at 0.02 mA cm^{-2}. For devices B and C, the corresponding peak efficiencies are η_{ext} = 8.23 %, η_L = 24.73 cd A^{-1}, and η_p = 15.54 lm W^{-1}, and η_{ext} = 7.72 %, η_L = 23.24 cd A^{-1}, and η_p = 16.23 lm W^{-1}, respectively. For **2**, the highest values achieved for η_{ext}, η_L, and η_p at the 5 wt.-% guest concentration (device D) are 7.89 %, 19.26 cd A^{-1} and 11.22 lm W^{-1}, respectively. The EL efficiency data for devices E and F are tabulated in Table 3. Figure 6 illustrates η_{ext} as a function of phosphor concentration for **1** and **2**. At the lower concentrations, the η_{ext} value increases with increasing concentrations of dopants. At high concentrations, above 5 wt.-%, η_{ext} tends to decrease, probably as a consequence of concentration quenching, and the maximum η_{ext} was achieved at 5 wt.-% concentration. As is the case for other

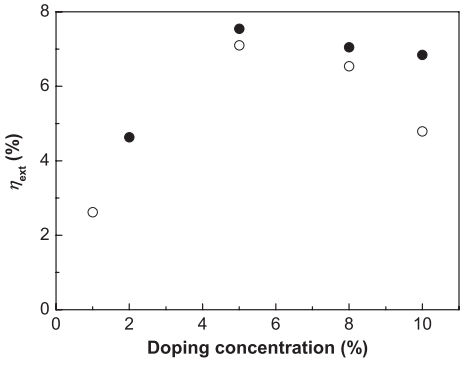

Figure 6. The external quantum efficiency (η_{ext}) of the electrophosphorescent OLED devices versus doping concentration of **1** (●) and **2** (○) at the constant current density of 1 mA cm^{-2}.

Ir^{III} emitters, the device efficiencies witnessed a decay with increasing driving voltage and current density. For **1**, at 5 wt.-% doping (device A) and a practical current density of 20 mA cm^{-2}, the external quantum efficiency is 4.58 % with a luminance efficiency of 13.81 cd A^{-1}, whereas at a higher current density of 100 mA cm^{-2}, the quantum and luminance efficiencies gradually drop to 2.79 % and 8.31 cd A^{-1}, respectively. This corresponds to a loss of 39 % in emission efficiency, and this kind of decrease has been discussed as arising from a triplet–triplet annihilation effect.[21] Almost the same percentage loss in η_{ext} was observed for devices B and C. Likewise, devices D–F suffered from a gradual loss of ca. 40–45 % in η_{ext} as the current density increases from 20 to 100 mA cm^{-2}.

3. Concluding Remarks

In summary, we have demonstrated for the first time the synthesis of iridium phosphor complexes based on a diphenylaminofluorene framework, and these complexes emit very strong yellow to orange color both in steady-state emissions and electrophosphorescence. Addition of pendant diarylamino moieties in these complexes can suppress the crystallinity of the materials for high efficiency. End-capping of the fluorene core with NPh_2 group in the phosphor has been shown to offer advantages in terms of lowering the first ionization potential, enhancing thermal stability, and inducing good amorphous morphological stability as compared to the neat 2-pyridinylfluorene congener, which makes them superior bifunctional phosphorescent materials. These improvements resulted in a high external quantum efficiency of up to nearly 10 % ph/el (photons per electron) that corresponds to luminance and power efficiencies of 30 cd A^{-1} and 21 lm W^{-1}, respectively, for the device prepared from [Ir(DPA-Flpy)$_3$] as the guest. The new triplet emitters reported here have the potential for further optimization by structural modifications of the ligand substituents to fine-tune both device color and efficiency.

4. Experimental

General Information: All reactions were performed under nitrogen. Solvents were carefully dried and distilled from appropriate drying agents prior to use. Commercially available reagents were used without further purification unless otherwise stated. The procedure for the synthesis of (7-bromo-9,9-diethylfluoren-2-yl)diphenylamine followed the methods reported in the literature [13]. All reactions were monitored by thin-layer chromatography (TLC) with Merck pre-coated glass plates. Compounds were visualized with UV light irradiation at 254 and 365 nm. Flash column chromatography and preparative TLC were carried out using silica gel from Merck (230–400 mesh). Fast-atom-bombardment (FAB) mass spectra were recorded on a Finnigan MAT SSQ710 system. NMR spectra were measured in $CDCl_3$ on a Varian Inova 400 MHz FT-NMR spectrometer; chemical shifts were quoted relative to the internal standard tetramethylsilane for ^1H and $^{13}C\{^1H\}$ NMR data.

Physical Measurements: UV-vis spectra were obtained on a HP-8453 spectrophotometer. The photoluminescent properties and lifetimes of the compounds were probed on the Photon Technology International (PTI) Fluorescence Master Series QM1 system. The phosphorescence quantum yields were determined in CH_2Cl_2 solutions at 293 K against *fac*-[Ir(ppy)$_3$] as a reference ($\Phi_P = 0.40$) [18]. For solid-state emission spectral measurements, the 325 nm line of a He–Cd laser was used as an excitation source. The luminescence spectra were analyzed by a 0.25 m focal length double monochromator with a Peltier-cooled photomultiplier tube and processed with a lock-in-amplifier. Electrochemical measurements were made using a BAS CV-50W model potentiostat. A conventional three-electrode configuration, consisting of a platinum working electrode, a Pt-wire counter electrode, and a Ag/AgCl reference electrode, was used. The solvent in all measurements was tetrahydrofuran (THF), and the supporting electrolyte was 0.1 M $[Bu_4N]PF_6$. Ferrocene was added as a calibrant after each set of measurements, and all potentials reported were quoted with reference to the ferrocene–ferrocenium (Fc/Fc^+) couple at a scan rate of 100 mV s^{-1}. Thermal analyses were performed with the Perkin-Elmer Pyris Diamond DSC and Perkin-Elmer TGA6 thermal analyzers.

Preparation of (9,9-Diethyl-7-pyridinylfluoren-2-yl)diphenylamine [H(DPA-Flpy)]: (7-Bromo-9,9-diethylfluoren-2-yl)diphenylamine (2.30 g, 4.91 mmol) and 2-(tributylstannyl)pyridine (2.07 g, 5.62 mmol) were mixed in dry toluene (50 mL) and $Pd(PPh_3)_4$ (0.58 g, 0.50 mmol) was then added to the solution. The resulting mixture was stirred at 110 °C for 24 h. After cooling to room temperature, the reaction mixture was poured into a separating funnel and CH_2Cl_2 (200 mL) was added followed by washing with water (3 × 100 mL). The organic phase was dried over $MgSO_4$. Solvent was then removed and the residue was purified by column chromatography eluting with CH_2Cl_2–hexane (3:1, v/v). The title product was obtained as a yellow solid (1.80 g, 79 %).

Spectral data: MS (FAB): *m/z* 466 (M^+). ^1H NMR (400 MHz, $CDCl_3$, 293 K): δ [ppm] 8.70 (d, J = 4.6 Hz, 1H, Ar), 7.98–7.58 (m, 6H, Ar), 7.27–6.97 (m, 13H, Ar), 2.07–1.91 (m, 4H, Et), 0.38 (t, J = 7.3 Hz, 6H, Et). $^{13}C\{^1H\}$ NMR (100.6 MHz, $CDCl_3$, 293 K): δ [ppm] 157.64, 151.71, 150.31, 149.44, 147.81, 147.30, 142.18, 137.31, 136.49, 135.98, 129.05, 125.81, 123.76, 123.44, 122.42, 121.60, 121.01, 120.54, 120.38, 119.15, 119.13, 56.27, 32.72, 8.71. Anal. calcd. for $C_{34}H_{30}N_2$: C, 87.52; H, 6.48; N, 6.00; found: C, 87.25; H, 6.26; N, 5.78.

*Preparation of [Ir(DPA-Flpy)$_3$] (**1**)*: [Ir(acac)$_3$] (0.15 g, 0.30 mmol) and [H(DPA-Flpy)] (0.50 g, 1.07 mmol) were mixed in glycerol (16 mL) under a N_2 atmosphere. The reaction mixture was heated to 220 °C for 18 h, after which time the mixture was cooled to room temperature and water (50 mL) was added. The resulting mixture was extracted with CH_2Cl_2 (3 × 100 mL) and the organic phase was dried over $MgSO_4$. Upon solvent removal under vacuum, the residue was purified by column chromatography using CH_2Cl_2 as eluent to afford the title compound as an orange solid (0.10 g, 21 %).

Spectral data: MS (FAB): *m/z* 1589 (M^+). ^1H NMR (400 MHz, $CDCl_3$, 293 K): δ [ppm] 7.91 (d, J = 8.1 Hz, 3H, Ar), 7.68 (d, J = 5.4 Hz, 3H, Ar), 7.58–7.52 (m, 6H, Ar), 7.20–6.77 (m, 45H, Ar), 1.97–1.82 (m, 12H, Et), 0.45–0.32 (m, 18H, Et). $^{13}C\{^1H\}$ NMR (100.6 MHz, $CDCl_3$, 293 K): δ [ppm] 167.00, 160.89, 152.11, 148.11, 147.15, 146.35, 142.91, 142.42, 141.30, 138.15, 135.40, 128.96, 127.79, 123.96, 123.17, 121.83, 121.00, 119.93, 118.81, 118.02, 55.34, 33.58, 32.61, 8.89, 8.63. Anal. calcd. for $C_{102}H_{87}N_6Ir$: C, 77.10; H, 5.52; N, 5.29; found: C, 76.98; H, 5.33; N, 5.02.

Preparation of [Ir(DPA-Flpy)$_2$Cl]$_2$: Ligand [H(DPA-Flpy)] (0.50 g, 1.07 mmol) and $IrCl_3 \cdot nH_2O$ (0.10 g, 54 wt.-% Ir content) were added to a mixture of 2-ethoxyethanol and water (10 mL, 3:1, v/v). The reaction mixture was stirred at 120 °C for 18 h and after cooling to room temperature, a yellow precipitate was obtained. The precipitate was collected and washed with ethanol (20 mL) and hexane (10 mL). Subsequently, the cyclometalated Ir dimer $[Ir(DPA\text{-}Flpy)_2Cl]_2$ was dried under vacuum and it was finally isolated as a yellow solid (0.28 g, 85 %) that was used for the next step without further purification.

Spectral data: ^1H NMR (400 MHz, $CDCl_3$, 293 K): δ [ppm] 9.36 (d, J = 5.4 Hz, 4H, Ar), 7.90 (d, J = 8.1 Hz, 4H, Ar), 7.79–7.71 (m, 4H, Ar), 7.38 (s, 4H, Ar), 7.25–6.78 (m, 56H, Ar), 6.23 (s, 4H, Ar), 1.85–1.69 (m, 16H, Et), 0.27–0.19 (m, 24H, Et). $^{13}C\{^1H\}$ NMR (100.6 MHz, $CDCl_3$, 293 K): δ [ppm] 168.87, 152.25, 147.98, 146.74, 144.55, 142.91, 141.99, 141.94, 136.60, 135.83, 129.01, 123.58, 123.28, 122.17, 121.35, 120.99,

ADVANCED FUNCTIONAL MATERIALS

120.14, 119.28, 118.12, 117.84, 109.77, 55.19, 32.82, 32.46, 8.76, 8.70. Anal. calcd. for $C_{136}H_{116}N_8Cl_2Ir_2$: C, 70.48; H, 5.04; N, 4.83; found: C, 70.24; H, 4.88; N, 4.50.

*Preparation of [Ir(DPA-Flpy)$_2$(acac)] (**2**)*: [Ir(DPA-Flpy)$_2$Cl]$_2$ (0.28 g, 0.12 mmol), Na_2CO_3 (0.12 g, 1.13 mmol) and acetylacetone (0.3 mL) were combined in 2-ethoxyethanol (16 mL) and the reaction mixture was heated to 110 °C for 18 h. After reaction, the mixture was cooled to room temperature and water (50 mL) was added. The yellow precipitate was collected, dried, and then purified with TLC plates using CH_2Cl_2–hexane (3:1, v/v) as eluent. The target product was obtained as an orange solid in 10 % yield (0.015 g).

Spectral data: MS (FAB): *m*/*z* 1222 (M^+). ^{1}H NMR (400 MHz, $CDCl_3$, 293 K): δ [ppm] 8.59 (d, J = 5.4 Hz, 2H, Ar), 7.90 (d, J = 8.1 Hz, 2H, Ar), 7.77–7.71 (m, 2H, Ar), 7.43 (s, 2H, Ar), 7.25–6.84 (m, 28H, Ar), 6.47 (s, 2H, Ar), 5.26 (s, 1H, acac), 1.90–1.73 (m, 14H, Et + Me), 0.37 (t, J = 6.7 Hz, 6H, Et), 0.17 (t, J = 6.7 Hz, 6H, Et). ^{13}C{^{1}H} NMR (100.6 MHz, $CDCl_3$, 293 K): δ [ppm] 184.55, 168.91, 152.38, 148.36, 148.02, 146.70, 146.16, 142.91, 142.36, 142.02, 136.99, 136.41, 129.02, 123.50, 123.40, 123.23, 122.15, 120.73, 120.42, 119.53, 118.36, 118.20, 100.38, 55.20, 32.95, 32.45, 28.83, 8.83, 8.61. Anal. calcd. for $C_{73}H_{65}N_4O_2Ir$: C, 71.72; H, 5.36; N, 4.58; found: C, 71.53; H, 5.05; N, 4.42.

OLED Fabrication and Measurements: Commercial indium tin oxide (ITO)-coated glass with sheet resistance of 20–30 Ω/square was used as the starting substrate. Before device fabrication, the ITO glass substrates were cleaned by ultrasonic baths in organic solvents followed by ozone treatment for 10 min. Each device was assembled in the following sequence: ITO on glass substrate (anode), 75 nm of NPB, 20 nm of the emitting layer made of CBP host and phosphorescent dopant (*x* %), 45 nm of TPBI, 1 nm of LiF, and 60 nm of Al (cathode). The organic layers were evaporated and laminated in the above sequence under 4×10^{-4} Pa without breaking vacuum between each vacuum deposition process. The emissive layer was formed by co-deposition of the dopant and the host. The evaporation rates were 1 ~ 2, 0.3, and 4 ~ 6 Å s^{-1} for organic materials, LiF, and aluminum, respectively. The layer thickness was monitored in situ using a quartz crystal oscillator. The active area of the device was 5 mm^2 as defined by the shadow mask. The electrical and optical characteristics of these devices were measured using R6145 DC voltage current source, FLUKE 45 dual display multimeter and Spectrascan PR650 spectrophotometer in a dark room under ambient air condition.

Received: August 8, 2005
Final version: November 17, 2005
Published online: March 6, 2006

[1] a) M. A. Baldo, D. F. O'Brien, Y. You, A. Shoustikov, S. Sibley, M. E. Thompson, S. R. Forrest, *Nature* **1998**, *395*, 151. b) M. A. Baldo, M. E. Thompson, S. R. Forrest, *Pure Appl. Chem.* **1999**, *71*, 2095. c) M. A. Baldo, M. E. Thompson, S. R. Forrest, *Nature* **2000**, *403*, 750. d) T. Tsutsui, M.-J. Yang, M. Yahiro, K. Nakamura, T. Watanabe, T. Tsuji, Y. Fukuda, T. Wakimoto, S. Miyaguchi, *Jpn. J. Appl. Phys. Part 2* **1999**, *38*, L1502.

[2] a) A. Köhler, J. S. Wilson, R. H. Friend, *Adv. Mater.* **2002**, *14*, 701. b) X. Gong, M. R. Robinson, J. C. Ostrowski, D. Moses, G. C. Bazan, A. J. Heeger, *Adv. Mater.* **2002**, *14*, 581. c) C. Adachi, M. A. Baldo, M. E. Thompson, S. R. Forrest, *J. Appl. Phys.* **2001**, *90*, 5048.

[3] a) S.-J. Yeh, M.-F. Wu, C.-T. Chen, Y.-H. Song, Y. Chi, M.-H. Ho, S.-F. Hsu, C. H. Chen, *Adv. Mater.* **2005**, *17*, 285. b) C.-L. Li, Y.-J. Su, Y.-T. Tao, P.-T. Chou, C.-H. Chien, C.-C. Cheng, R.-S. Liu, *Adv. Funct. Mater.* **2005**, *15*, 387. c) D. K. Rayabarapu, B. M. J. S. Paulose, J.-P. Duan, C.-H. Cheng, *Adv. Mater.* **2005**, *17*, 349. d) Y.-H. Song, S.-J. Yeh, C.-T. Chen, Y. Chi, C.-S. Liu, J.-K. Yu, Y.-H. Hu, P.-T. Chou, S.-M. Peng, G.-H. Lee, *Adv. Funct. Mater.* **2004**, *14*, 1221. e) H. Z. Xie, M. W. Liu, O. Y. Wang, X. H. Zhang, C. S. Lee, L. S. Hung, S. T. Lee, P. F. Teng, H. L. Kwong, H. Zheng, C. M. Che, *Adv. Mater.* **2001**, *13*, 1245. f) J. M. Lupton, I. D. W. Samuel, M. J. Frampton, R. Beavington, P. L. Burn, *Adv. Funct. Mater.* **2001**, *11*, 287. g) C.-L. Lee, R. R. Das, J.-J. Kim, *Chem. Mater.* **2004**, *16*, 4642. h) M. K. Nazeeruddin, R. Humphry-Baker, D. Berner, S. Rivier, L. Zuppiroli, M. Graetzel, *J. Am. Chem. Soc.* **2003**, *125*, 8790. i) H.-C. Li, P.-T. Chou, Y.-H. Hu, Y.-M. Cheng, R.-S. Liu, *Organometallics* **2005**, *24*, 1329. j) K. R. Justin Thomas, M. Velusamy, J. T. Lin, C.-H. Chien, Y.-T. Tao, Y. S. Wen, Y.-H. Hu, P.-T. Chou, *Inorg. Chem.* **2005**, *44*, 5677. k) W.-S. Huang, J.-T. Lin, C.-H. Chien, Y.-T. Tao, S.-S. Sun, Y.-S. Wen, *Chem. Mater.* **2004**, *16*, 2480.

[4] a) V. Adamovich, J. Brooks, A. Tamayo, A. M. Alexander, P. I. Djurovich, B. W. D'Andrade, C. Adachi, S. R. Forrest, M. E. Thompson, *New J. Chem.* **2002**, *26*, 1171. b) C.-M. Che, S.-C. Chan, H.-F. Xiang, M. C. W. Chan, Y. Liu, Y. Wang, *Chem. Commun.* **2004**, 1484. c) W. Lu, B.-X. Mi, M. C. W. Chan, Z. Hui, C.-M. Che, N. Zhu, S.-T. Lee, *J. Am. Chem. Soc.* **2004**, *126*, 4958. d) S.-C. Chan, M. C. W. Chan, Y. Wang, C.-M. Che, K.-K. Cheung, N. Zhu, *Chem. Eur. J.* **2001**, *7*, 4180. e) J. Kavitha, S.-Y. Chang, Y. Chi, J.-K. Yu, Y.-H. Hu, P.-T. Chou, S.-M. Peng, G.-H. Lee, Y.-T. Tao, C.-H. Chien, A. J. Carty, *Adv. Funct. Mater.* **2005**, *15*, 223. f) W.-Y. Wong, Z. He, S.-K. So, K.-L. Tong, Z. Lin, *Organometallics* **2005**, *24*, 4079.

[5] a) Y.-H. Niu, Y.-L. Tung, Y. Chi, C.-F. Shu, J. H. Kim, B. Chen, J. Luo, A. J. Carty, A. K.-Y. Jen, *Chem. Mater.* **2005**, *17*, 3532. b) X. Jiang, A. K.-Y. Jen, B. Carlson, L. R. Dalton, *Appl. Phys. Lett.* **2002**, *81*, 3125. c) B. Carlson, G. D. Phelan, W. Kaminsky, L. Dalton, X. Z. Jiang, S. Liu, A. K.-Y. Jen, *J. Am. Chem. Soc.* **2002**, *124*, 14 162. d) S. Bernhard, X. Gao, G. G. Malliaras, H. D. Abruna, *Adv. Mater.* **2002**, *14*, 433. e) Y. Ma, H. Zhang, J. Shen, C. Che, *Synth. Met.* **1998**, *94*, 245. f) Y.-L. Tung, S.-W. Lee, Y. Chi, Y.-T. Tao, C.-H. Chien, Y.-M. Cheng, P.-T. Chou, S.-M. Peng, C.-S. Liu, *J. Mater. Chem.* **2005**, *15*, 460.

[6] Y.-L. Tung, S.-W. Lee, Y. Chi, L.-S. Chen, C.-F. Shu, F.-I. Wu, A. J. Carty, P.-T. Chou, S.-M. Peng, G.-H. Lee, *Adv. Mater.* **2005**, *17*, 1059.

[7] a) I. R. Laskar, T.-M. Chen, *Chem. Mater.* **2004**, *16*, 111. b) T. Tsuzuki, N. Shirasawa, T. Suzuki, S. Tokito, *Adv. Mater.* **2003**, *15*, 1455. c) P. Coppo, E. A. Plummer, L. De Cola, *Chem. Commun.* **2004**, 1774. d) T.-H. Kwon, H. S. Cho, M. K. Kim, J.-W. Kim, J.-J. Kim, K. H. Lee, S. J. Park, I.-S. Shin, H. Kim, D. M. Shin, Y. K. Chung, J.-I. Hong, *Organometallics* **2005**, *24*, 1578. e) F. Neve, M. L. Deda, A. Crispini, A. Bellusci, F. Puntoriero, S. Campagna, *Organometallics* **2004**, *23*, 5856.

[8] a) A. Kraft, A. C. Grimsdale, A. B. Holmes, *Angew. Chem. Int. Ed.* **1998**, *37*, 402. b) J. G. C. Veinot, T. J. Marks, *Acc. Chem. Res.* **2005**, *38*, 632. c) J. L. Segura, *Acta Polym.* **1998**, *49*, 319.

[9] a) X. Gong, M. R. Robinson, J. C. Ostrowski, D. Moses, G. C. Bazan, A. J. Heeger, *Adv. Mater.* **2002**, *14*, 581. b) X. Gong, J. C. Ostrowski, D. Moses, G. C. Bazan, A. J. Heeger, *Adv. Funct. Mater.* **2003**, *13*, 439. c) X. Gong, J. C. Ostrowski, G. C. Bazan, D. Moses, A. J. Heeger, M. S. Liu, A. K.-Y. Jen, *Adv. Mater.* **2003**, *15*, 45. d) F.-I. Wu, H.-J. Su, C.-F. Shu, L. Luo, W.-G. Diau, C.-H. Cheng, J.-P. Duan, G.-H. Lee, *J. Mater. Chem.* **2005**, *15*, 1035. e) A. J. Sandee, C. K. Williams, N. R. Evans, J. E. Davies, C. E. Boothby, A. Köhler, R. H. Friend, A. B. Holmes, *J. Am. Chem. Soc.* **2004**, *126*, 7041.

[10] a) D. Neher, *Macromol. Rapid Commun.* **2001**, *22*, 1365. b) W.-Y. Wong, *Coord. Chem. Rev.* **2005**, *249*, 971.

[11] a) P. Strohriegl, J. V. Grazulevicius, *Adv. Mater.* **2002**, *14*, 1439. b) R. D. Hreha, C. P. George, A. Haldi, B. Domercq, M. Malagoli, S. Barlow, J.-L. Brédas, B. Kippelen, S. R. Marder, *Adv. Funct. Mater.* **2003**, *13*, 967. c) P. Kunda, K. R. Justin Thomas, J. T. Lin, Y.-T. Tao, C.-H. Chien, *Adv. Funct. Mater.* **2003**, *13*, 445.

[12] K.-T. Wong, Z.-J. Wang, Y.-Y. Chien, C.-L. Wang, *Org. Lett.* **2001**, *3*, 2285.

[13] R. Kannan, G. S. He, L. Yuan, F. Xu, P. N. Prasad, A. G. Dombroskie, B. A. Reinhardt, J. W. Baur, R. A. Waia, L.-S. Tan, *Chem. Mater.* **2001**, *13*, 1896.

[14] a) A. B. Tamayo, B. D. Alleyne, P. I. Djurovich, S. Lamansky, I. Tsyba, N. N. Ho, R. Bau, M. E. Thompson, *J. Am. Chem. Soc.* **2003**, *125*, 7377. b) S. Lamansky, P. Djurovich, D. Murphy, F. Abdel-Razzaq,

ADVANCED FUNCTIONAL MATERIALS

H.-E. Lee, C. Adachi, P. E. Burrows, S. R. Forrest, M. E. Thompson, *J. Am. Chem. Soc.* **2001**, *123*, 4304. c) S. Lamansky, P. Djurovich, D. Murphy, F. Abdel-Razzaq, R. Kwong, I. Tsyba, M. Bortz, B. Mui, R. Bau, M. E. Thompson, *Inorg. Chem.* **2001**, *40*, 1704. d) S. Okada, K. Okinaka, H. Iwawaki, M. Furugori, M. Hashimoto, T. Mukaide, J. Kamatani, S. Igawa, A. Tsuboyama, T. Takiguchi, K. Ueno, *Dalton Trans.* **2005**, 1583.

[15] J. C. Ostrowski, M. R. Robinson, A. J. Heeger, G. C. Bazan, *Chem. Commun.* **2002**, 784.

[16] P. J. Low, M. A. J. Paterson, A. E. Goeta, D. S. Yufit, J. A. K. Howard, J. C. Cherryman, D. R. Tackley, B. Brown, *J. Mater. Chem.* **2004**, *14*, 2516.

[17] A. Tsuboyama, H. Iwawaki, M. Furugori, T. Mukaide, J. Kamatani, S. Igawa, T. Moriyama, S. Miura, T. Takiguchi, S. Okada, M. Hoshino, K. Ueno, *J. Am. Chem. Soc.* **2003**, *125*, 12 971.

[18] K. A. King, P. J. Spellane, R.-J. Watts, *J. Am. Chem. Soc.* **1985**, *107*, 1431.

[19] M. Thelakkat, H.-W. Schmidt, *Adv. Mater.* **1998**, *10*, 219.

[20] a) K. M.-C. Wong, X. Zhu, L.-L. Hung, N. Zhu, V. W.-W. Yam, H.-S. Kwok, *Chem. Commun.* **2005**, 2906. b) J.-P. Duan, P.-P. Sun, C.-H. Cheng, *Adv. Mater.* **2003**, *15*, 224. c) C. H. Chen, J. Shi, C. W. Tang, *Macromol. Symp.* **1997**, *125*, 1.

[21] M. A. Baldo, C. Adachi, S. R. Forrest, *Phys. Rev. B* **2000**, *62*, 10 967.